Applied Physics Letters

Exquisite growth control and magnetic properties of yttrium iron garnet thin films

Cite as: Appl. Phys. Lett. **108**, 102403 (2016); https://doi.org/10.1063/1.4943210
Submitted: 16 December 2015 . Accepted: 14 February 2016 . Published Online: 08 March 2016

Chi Tang, Mohammed Aldosary, Zilong Jiang, Houchen Chang, Benjamin Madon, Kyle Chan, Mingzhong Wu, Javier E. Garay, and Jing Shi

Exquisite growth control and magnetic properties of yttrium iron garnet thin films

Chi Tang,[1] Mohammed Aldosary,[1] Zilong Jiang,[1] Houchen Chang,[2] Benjamin Madon,[3] Kyle Chan,[4] Mingzhong Wu,[2] Javier E. Garay,[4] and Jing Shi[1]
[1]*Department of Physics and Astronomy, University of California, Riverside, California 92521, USA*
[2]*Department of Physics, Colorado State University, Fort Collins, Colorado 80523, USA*
[3]*Laboratoire des Solides Irradiés, Ecole Polytechnique, CNRS, CEA, Université Paris-Saclay, F 91128 Palaiseau, France*
[4]*Department of Mechanic Engineering and Materials Science & Engineering Program, University of California, Riverside, California 92521, USA*

(Received 16 December 2015; accepted 14 February 2016; published online 8 March 2016)

A layer-by-layer epitaxial growth up to 227 atomic layers of ferrimagnetic insulator yttrium iron garnet (YIG) thin films is achieved on (110)-oriented gadolinium gallium garnet substrates using pulsed laser deposition. Atomically smooth terraces are observed on YIG films up to 100 nm in thickness. The root-mean-square roughness is as low as 0.067 nm. The easy-axis lies in the film plane, indicating the dominance of shape anisotropy. For (110)-YIG films, there is well-defined two-fold in-plane anisotropy, with the easiest axis directed along [001]. The Gilbert damping constant is determined to be 1.0×10^{-4} for 100 nm thick films. © *2016 AIP Publishing LLC*.
[http://dx.doi.org/10.1063/1.4943210]

Since 1960s the rare-earth iron garnet bulk materials have been extensively explored owing to their unique spin dynamic and magneto-optical properties. Among all members of magnetic garnet family, yttrium iron garnet ($Y_3Fe_5O_{12}$ or YIG) has attracted the most attention for its extremely low damping[1] ($\sim 3 \times 10^{-5}$) combined with the low infrared absorption and the large Verdet constant[2] desired for applications such as Faraday rotators, isolators, and sensors.[3,4] A surge in the research of YIG thin films for spintronics started recently. Compared with other magnetic insulators such as EuS and EuO, YIG has a high Curie temperature (~550 °C) and a large band gap[5] (~2.85 eV); therefore, it is an excellent room-temperature pure spin current source for spin Seebeck effect[6] and spin pumping.[7–11] YIG can induce ferromagnetism in adjacent non-magnetic films or causes peculiar magnetoresistance phenomena.[12–15] In novel heterostructures constructed with YIG and graphene or topological insulators,[16,17] the exchange interaction is expected to modify electron's Dirac spectrum. In addition, recent experiments on both lateral and vertical structures have demonstrated that magnons in YIG can mediate nonlocal transport effects.[18,19] Unlike in bulk crystal applications, thin film devices rely on interactions across the interface; therefore, the surface properties (e.g., morphology and magnetism) are extremely important. Pulsed laser deposition (PLD) is a common technique for oxide thin film growth. However, systematic studies of YIG growth and correlation between the structural and magnetic properties are relatively scarce. In this report, we demonstrate an exquisite control of (110)-oriented YIG film growth with PLD. By maintaining the layer-by-layer growth, the ultra-smooth atomic terraces are obtained. We show that the YIG films have in-plane uniaxial anisotropy and extremely low Gilbert damping constant.

YIG powder purchased from Alfa Aesar is densified via the current activated pressure assisted densification (CAPAD) processing technique[20] at 950 °C with an applied load of 100 MPa for 5 min. The final relative density of the target is over 85%, and the crystal structure of YIG target is confirmed by x-ray diffraction. The commercially available GGG(110) substrates are rinsed sequentially with acetone, isopropyl alcohol, and DI water, and then annealed in oxygen at 1000 °C for 6 h. As discussed in detail later, because of this substrate treatment, an atomically terraced gadolinium gallium garnet (GGG) surface emerges, enabling the subsequent ultra-flat terraced YIG film growth. The substrates are *in situ* baked with a base pressure around 5×10^{-7} Torr at ~200 °C for 5 h. Before deposition, the substrates are then annealed at ~750 °C under a 1.5 mTorr oxygen pressure with 12 wt. % ozone for 30 min. During the pre-deposition annealing, the reflection high-energy electron diffraction (RHEED) spots become sharper and brighter, and the intensity saturates after 30 min annealing. Then, under the same condition of oxygen and temperature as the pre-deposition annealing, the KrF excimer laser pulses of 248 nm in wavelength with power of 150 mJ strike the target at a repetition frequency of 1 Hz. The differentially pumped RHEED is kept on to monitor the growth of YIG layers *in situ*. As shown in Fig. 1(a), 227 continuous RHEED intensity oscillations are observed before the termination of growth, showing excellent layer-by-layer epitaxial growth of YIG. The oscillation period of 300 s represents growth of one atomic layer along the (110) direction of the cubic cell of GGG with the lattice constant of 12.383 Å. The layer-by-layer growth obtained with such a low repetition rate is below the threshold found in a previous report.[21] The film thickness is calculated to be ~100 nm, which is further confirmed by the atomic force microscopy (AFM) and a Dektak profilometer, and the film growth rate is 0.09 nm/min. Fig. 1(b) shows a few zoom-in RHEED oscillations. Fig. 1(c) is the RHEED pattern of the as-grown YIG film, which shows the identical cubic crystalline structure to that of GGG with negligible lattice mismatch. The Kikuchi lines from the

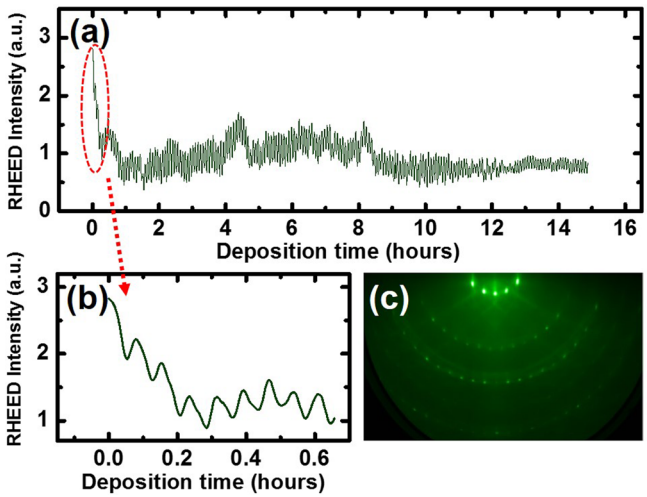

FIG. 1. (a) 227 layers (100 nm) thick YIG film of continuous layer by layer RHEED oscillations observed during the growth on (110) GGG substrate using the pulsed laser deposition technique. (b) Zoom-in data of RHEED oscillations for a chosen time slot. (c) RHEED pattern of YIG film showing single crystalline structure of YIG after deposition.

diffraction of diffusely scattered electrons[22] are also clearly resolved, confirming that the YIG film is of high crystallinity.

The atomically flat substrate surface is essential for obtaining high-quality growth of epitaxial film on top. The surface quality is monitored by the atomic terrace formation upon treatment. A wide range of annealing temperatures (from 400 to 1300 °C) has been explored to study the effect of annealing, and the results are summarized in Figs. 2(a)–2(c). Fig. 2(a) shows the surface morphology of a purchased GGG substrate right after cleaning but without annealing. The root-mean-square (RMS) roughness is 0.51 nm. After annealing in oxygen at 1000 °C for 6 h, atomic terraces emerge as shown in Fig. 2(b). Similar results were previously found on annealed STO substrates.[23,24] In the meantime, the RMS roughness is greatly reduced down to 0.15 nm. However, when the annealing temperature is increased to 1100 °C for the same amount of time, pits and cracks appear on the entire substrate, even though the RMS roughness is only increased slightly. Figs. 2(a)–2(c) display the dramatic effect of annealing on the GGG substrates. Annealing temperature needs to be sufficiently high to promote atomic mobility to reduce roughness but sufficiently low to keep the stoichiometry (preventing volatilization of ions) in the film. The optimized temperature, 1000 °C is 0.63 of the melting T_m. At this temperature, one would expect volume diffusion to be active. It is likely that 1100 °C ($T/T_m = 0.69$) causes too much long-range diffusion or volatilization. For comparison, Fig. 2(d) is the surface profile for a 30 nm thick YIG film. Extremely smooth atomic terraces with roughness 0.067 nm are evidently resulted, due to the layer-by-layer growth mode that preserves the excellent initial surface morphology. We emphasize that maintaining such long RHEED oscillations during the entire growth is essential for obtaining the atomically smooth terraces with the lowest surface roughness of YIG films. Fig. 2(e) shows a transmission electron microscopy (TEM) image of the 30 nm YIG film grown on GGG(110), indicating a sharp interface with negligible mismatch between YIG and GGG. The atomically resolved YIG layers show the epitaxy, consistent with the previous RHEED results.

YIG hysteresis loops are measured using a vibrating sample magnetometer (VSM) with both out-of-plane and in-plane field orientations, as shown in Fig. 3. Fig. 3(a) is a top view of the YIG sample marked with main crystallographic orientations. The two edges of (110)-orientated GGG substrate are confirmed to be along $[1\bar{1}\bar{1}]$ and $[1\bar{1}2]$. $[1\bar{1}1]$, another member of the 111 family, lies at an angle of 70° with respect to the $[1\bar{1}\bar{1}]$ edge. YIG films grown on GGG have the easy axis lying in the film plane shown in Fig. 3(b), due to the dominance of shape anisotropy.[25,26] The

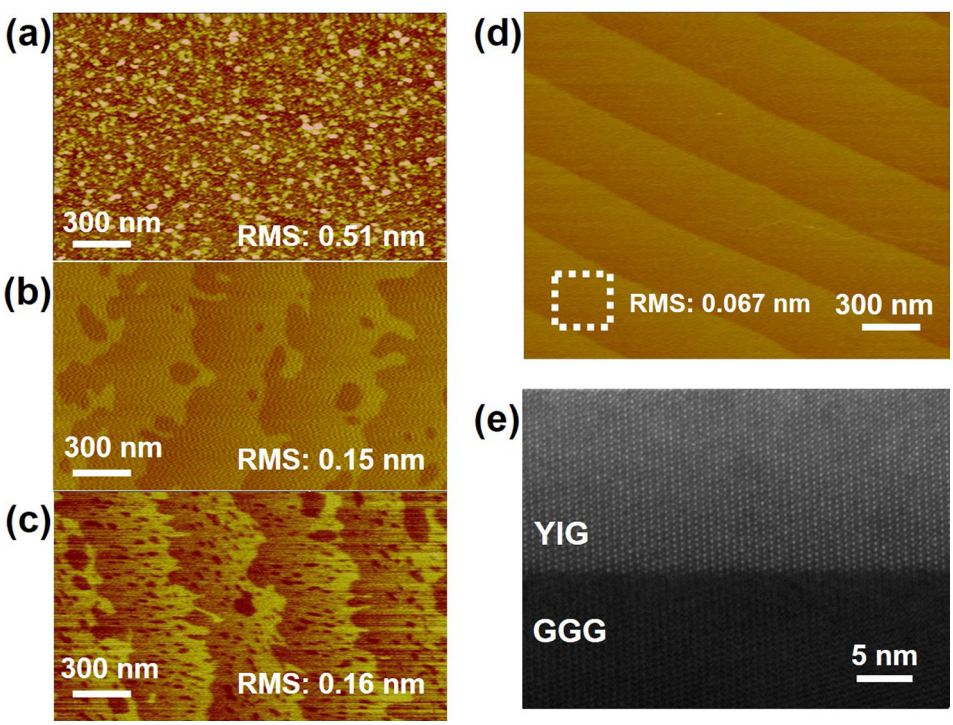

FIG. 2. (a) AFM surface morphology of GGG substrates after different surface treatments. Top: original purchased GGG substrates after ultrasonicated in acetone and isopropanol for surface cleaning. (b) Annealed GGG substrates at 1000 °C in O_2 environment for 6 h. (c) Annealed GGG substrates at 1100 °C in O_2 environment for 6 h. (d) AFM surface morphology of 30 nm thick YIG film on the (110) GGG substrates. (e) TEM image of a 30 nm thick YIG thin film on (110) the GGG substrate.

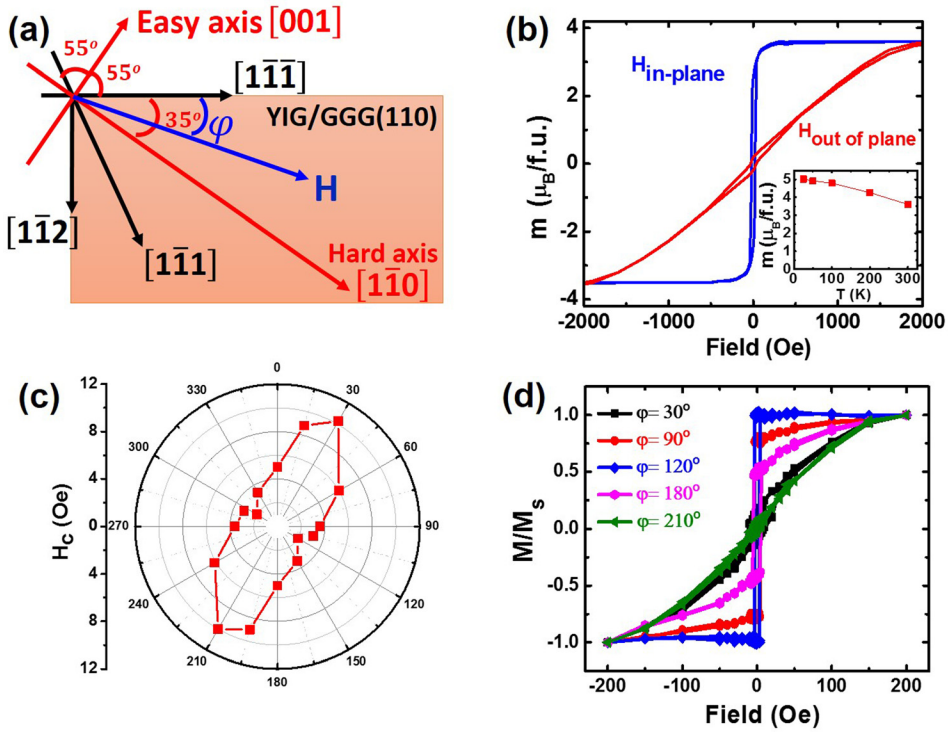

FIG. 3. (a) Coordinate system of YIG film plane with the orientations of crystalline directions. (b) Magnetic hysteresis loop measurements of 30 nm thick YIG film on (110) GGG with field out of plane (red) and in film plane (blue) at 300 K. Inset: A temperature dependence of saturation magnetization in unit of μ_B per formula unit. (c) Azimuth angle dependence of coercive field. (d) In-plane angle rotation of magnetic hysteresis loops showing in-plane two fold symmetry of the (110) oriented YIG film.

saturation moment is found to be $3.5\mu_B$ per formula unit at room temperature and reaches approximately $5\mu_B$ at 10 K. Aside from the strong in-plane anisotropy, the (110)-oriented YIG film shows two-fold symmetry in the film plane, as indicated in Figs. 3(c) and 3(d). The azimuth angle φ is measured between the external field H and the $[1\bar{1}\bar{1}]$ edge. Fig. 3(d) is the in-plane magnetic hysteresis loops for a few selected φ angles, showing an in-plane easy axis oriented at $\varphi = 30°$ and an in-plane hard axis along the orthogonal direction, i.e., $\varphi = 120°$. The azimuth angular dependence of the coercive field is illustrated in Fig. 3(c), showing a clear in-plane uniaxial symmetry. The observed in-plane uniaxial anisotropy is obviously related to the crystalline structure of the (110)-oriented YIG film. In bulk YIG, 111 and $1\bar{1}0$ are the easiest and hardest axes, respectively.[27] In the film plane of (110)-oriented YIG, there are two equivalent axes from the 111 family, and the [001] axis lies in between these two axes about 55° from each. As a consequence,[28] [001] becomes the in-plane easy axis, and $[1\bar{1}0]$, about 35° from the $[1\bar{1}\bar{1}]$ edge and perpendicular to $[1\bar{1}0]$, becomes the in-plane hard axis, which corresponds well to $\varphi = 30°$ found in experiments. The torque measurements on flux-grown magnetic garnets also exhibit similar noncubic anisotropy, which was interpreted in terms of a growth induced pair-ordering model.[25]

Ferromagnetic resonance (FMR) measurements are performed on YIG films with different thicknesses. As shown in Fig. 4(a), a vector network analyzer (VNA) is used to measure the transmission signal through a low-loss coplanar waveguide transmission line with the YIG samples placed in the center. We obtain the frequency linewidth by fitting the FMR spectrum to a Lorentzian and then calculate the corresponding field linewidth,[29] which is plotted in Fig. 4(b). Both the intrinsic Gilbert damping constant α from the slope and the inhomogeneity linewidth broadening ΔH_0 from the

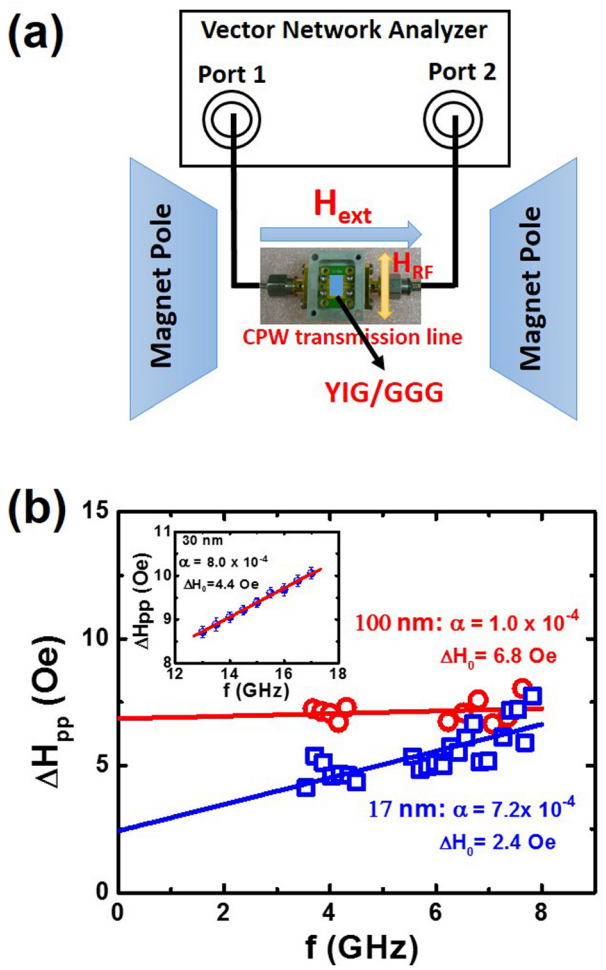

FIG. 4. (a) Schematic diagram of the VNA FMR transmission line measurement setup. (b) Excitation frequency dependence of FMR absorption linewidth for 100 nm and 17 nm thick YIG films. Inset: Frequency dependence of FMR absorption linewidth for the 30 nm thick YIG film measured using a Ku band shorted waveguide with a higher frequency range.

intercept can be extracted. The damping constant α for 100 nm thick YIG is $\sim 1.0 \times 10^{-4}$, among the best reported values of nm-thick YIG films,[25,30] and with a moderate $\Delta H_0 = 6.8$ Oe. The 17 nm YIG sample has a slightly larger value of $\alpha = 7.2 \times 10^{-4}$ and a smaller $\Delta H_0 = 2.4$ Oe. The FMR measurements are also extended to a higher frequency range using the Ku band shorted waveguide, and the Gilbert damping constant is determined to be from 7.0×10^{-4} to 1.0×10^{-3}, for YIG films with different thicknesses (15–30 nm), consistent with the VNA FMR measurements. The high-frequency result of a typical 30 nm thick YIG film is shown in the inset of Fig. 4(b). The increased Gilbert damping constant in thin films compared with that of the bulk ($\sim 3 \times 10^{-5}$) can be understood as a result of interface-defect associated two-magnon scattering[31–34] in ultrathin films. The increased damping in the nanometer-thick YIG films significantly shortens the spin wave propagation length[18,35,36] down to tens of μm compared to the mm scale of bulk YIG.[37]

In summary, we have demonstrated an exquisite control of YIG film growth using PLD. Single crystal YIG films have been epitaxially grown layer by layer up to 227 atomic layers continuously. Under the optimized sample treatment and growth, atomic terraces emerge in (110)-YIG films over a large range of thicknesses, thanks to the layer-by-layer growth mode. (110)-YIG films show a well-defined uniaxial in-plane anisotropy. The extremely low damping constant from the FMR measurements confirms the superb quality of YIG films resulted from the distinct growth mode.

We would like to thank T. Lin, X. Ma, M. Ranjbar, A. Khitun, and E. Li for many helpful discussions and their technical assistance. The work was supported as part of the SHINES, an Energy Frontier Research Center funded by the U.S. Department of Energy, Office of Science, Basic Energy Sciences under Award No. # SC0012670.

[1]M. Sparks, *Ferromagnetic-Relaxation Theory* (McGraw Hill, New York, 1964).
[2]K. T. V. Grattan and B. T. Meggitt, Opt. Fiber Sens. Technol. **2**, 214 (1999).
[3]M. N. Deeter, A. H. Rose, and G. W. Day, J. Lightwave Technol. **8**, 1838 (1990).
[4]B. J. H. Stadler and T. Mizumoto, IEEE Photonics J. **6**, 1 (2014).
[5]X. Jia, K. Liu, K. Xia, and G. E. Bauer, Eur. Phys. Lett. **96**, 17005 (2011).
[6]K. Uchida, J. Xiao, H. Adachi, J. Ohe, S. Takahashi, J. Ieda, T. Ota, Y. Kajiwara, H. Umezawa, H. Kawai, G. E. Bauer, S. Maekawa, and E. Saitoh, Nat. Mater. **9**, 894 (2010).
[7]C. W. Sandweg, Y. Kajiwara, K. Ando, E. Saitoh, and B. Hillebrands, Appl. Phys. Lett. **97**, 252504 (2010).
[8]L. H. Vilela-Leão, C. Salvador, A. Azevedo, and S. M. Rezende, Appl. Phys. Lett. **99**, 102505 (2011).
[9]B. Heinrich, C. Burrowes, E. Montoya, B. Kardasz, E. Girt, Y.-Y. Song, Y. Sun, and M. Wu, Phys. Rev. Lett. **107**, 066604 (2011).
[10]H. L. Wang, C. H. Du, Y. Pu, R. Adur, P. C. Hammer, and F. Y. Yang, Phys. Rev. Lett. **112**, 197201 (2014).
[11]V. Castel, N. Vlietstra, B. J. van Wees, and J. B. Youssef, Phys. Rev. B **86**, 134419 (2012).
[12]S. Y. Huang, X. Fan, D. Qu, Y. P. Chen, W. G. Wang, J. Wu, T. Y. Chen, J. Q. Xiao, and C. L. Chien, Phys. Rev. Lett. **109**, 107204 (2012).
[13]H. Nakayama, M. Althammer, Y.-T. Chen, K. Uchida, Y. Kajiwara, D. Kikuchi, T. Ohtani, S. Geprägs, M. Opel, S. Takahashi, R. Gross, G. E. W. Bauer, S. T. B. Goennenwein, and E. Saitoh, Phys. Rev. Lett. **110**, 206601 (2013).
[14]T. Lin, C. Tang, and J. Shi, Appl. Phys. Lett. **103**, 132407 (2013).
[15]T. Lin, C. Tang, H. M. Alyahayaei, and J. Shi, Phys. Rev. Lett. **113**, 037203 (2014).
[16]Z. Wang, C. Tang, and J. Shi, Phys. Rev. Lett. **114**, 016603 (2015).
[17]Z. Jiang, C.-Z. Chang, C. Tang, P. Wei, J. S. Moodera, and J. Shi, Nano. Lett. **15**, 5835 (2015).
[18]L. J. Cornelissen, J. Liu, R. A. Duine, J. B. Youssef, and B. J. van Wees, Nat. Phys. **11**, 1022 (2015).
[19]J. Li, Y. Xu, M. Aldosary, C. Tang, Z. Lin, S. Zhang, R. Lake, and J. Shi, Nat. Commun. **7**, 10858 (2016).
[20]J. E. Garay, Annu. Rev. Mater. Res. **40**, 445 (2010).
[21]Y. Krockenberger, K.-S. Yun, T. Hatano, S. Arisawa, M. Kawasaki, and Y. Tokura, J. Appl. Phys. **106**, 123911 (2009).
[22]A. Ichimiya and P. I. Cohen, *Reflection High-Energy Electron Diffraction* (Cambridge University Press, Cambridge, 2004).
[23]J. X. Ma, X. F. Liu, T. Lin, G. Y. Gao, J. P. Zhang, W. B. Wu, X. G. Li, and J. Shi, Phys. Rev. B **79**, 174424 (2009).
[24]W. Yuan, Y. Zhao, C. Tang, T. Su, Q. Song, J. Shi, and W. Han, Appl. Phys. Lett. **107**, 022404 (2015).
[25]H. Chang, P. Li, W. Zhang, T. Liu, A. Hoffmann, L. Deng, and M. Wu, IEEE Magn. Lett. **5**, 6700104 (2014).
[26]M. C. Onbasli, A. Kehlberger, D. H. Kim, G. Jakob, M. Kläui, A. V. Chumak, B. Hillebrands, and C. A. Ross, APL Mater. **2**, 106102 (2014).
[27]A. Rosencwaig, W. J. Tabor, F. B. Hagedorn, and L. G. Van Uitert, Phys. Rev. Lett. **26**, 775 (1971).
[28]B. D. Cullity, *Introduction to Magnetic Materials* (Addison-Wesley, Reading, Massachusetts, 1972).
[29]Y. Wei, S. L. Chin, and P. Svedlindh, J. Phys. D: Appl. Phys. **48**, 335005 (2015).
[30]H. Kurebayashi, O. Dzyapko, V. E. Demidov, D. Fang, A. J. Ferguson, and S. O. Demokritov, Nat. Mater. **10**, 660 (2011).
[31]R. Arias and D. L. Mills, Phys. Rev. B **60**, 7395 (1999).
[32]A. Azevedo, A. B. Oliveira, F. M. de Aguiar, and S. M. Rezende, Phys. Rev. B **62**, 5331 (2000).
[33]Y. Sun, Y.-Y. Song, H. Chang, M. Kabatek, M. Jantz, W. Schneider, M. Wu, H. Schultheiss, and A. Hoffmann, Appl. Phys. Lett. **101**, 152405 (2012).
[34]M. B. Jungfleisch, A. V. Chumak, A. Kehlberger, V. Lauer, D. H. Kim, M. C. Onbasli, C. A. Ross, M. Kläui, and B. Hillebrands, Phys. Rev. B **91**, 134407 (2015).
[35]P. Pirro, T. Brächer, A. V. Chumak, B. Lägel, C. Dubs, O. Surzhenko, P. Görnert, B. Leven, and B. Hillebrands, Appl. Rev. Lett. **104**, 012402 (2014).
[36]X. Ma, C. Tang, K. An, K. Olsson, K. Sobotkiewich, J. Li, J. Shi, and X. Li, "Complementary Methods of Characterizing Magnetic Damping in Yttrium Iron Garnet Thin Films Based on Brillouin Light Scattering," J. Appl. Phys. (submitted).
[37]T. Schneider, A. A. Serga, B. Leven, B. Hillebrands, R. L. Stamps, and M. P. Kostylev, Appl. Phys. Lett. **92**, 022505 (2008).